Menemui Matematik
(Discovering Mathematics)

journal homepage: https://persama.org.my/dismath/home

The Mathematical Modelling of Heat Transfer Properties in Kerosene-Based Nanofluid Flow with the Nanoparticles Composite: Alumina, Copper, and Graphene

Nanthini Balakrishnan[1], Ismasyazwi Ismaputera[2], Shahanaz Parvin[3] and Siti Suzilliana Putri Mohamed Isa[1,4*]

[1]*Institute for Mathematical Research, Universiti Putra Malaysia, 43400 UPM Serdang, Selangor, Malaysia*
[2]*Department of Mathematics, Faculty of Science, Universiti Putra Malaysia, 43400 UPM Serdang, Selangor, Malaysia*
[3]*Government Barhamganj College, Shibchar, Madaripur, Bangladesh*
[4]*Centre for Foundation Studies in Science of Universiti Putra Malaysia, Universiti Putra Malaysia, 43400 UPM Serdang, Selangor, Malaysia*

[1, 4]ctsuzilliana@upm.edu.my
*Corresponding author

Received: 21 October 2025
Accepted: 18 December 2025

ABSTRACT

Kerosene-based nanofluid offers better fuel enhancement and for high-temperature applications as they improve combustion efficiency and reduce emissions. Moreover, kerosene-based nanofluids perform better in high-temperature applications due to their higher boiling point and thermal stability. Besides, the nanoparticle types involved have their own specialization: graphene offers superior thermal and electrical conductivity, copper is appropriate for the fuel additives or conductive coatings, and the applications in the wear resistance, insulation, and ceramics are suited by alumina. Therefore, this paper investigates the boundary layer flow and heat transfer characteristics of a ternary hybrid nanofluid composed of alumina (Al_2O_3), copper (Cu), and graphene nanoparticles dispersed in kerosene oil over an exponentially shrinking permeable sheet. The research examines the effects of suction, velocity slip, thermal slip, and radiation on flow behaviour and heat transfer rate. The governing momentum and thermal energy equations are formulated using boundary layer theory and transformed into a system of ordinary differential equations through similarity transformation techniques. Numerical solutions are obtained using MATLAB to analyse the variation of the physical parameters and the related distributions such as the skin friction coefficient and local Nusselt number. Results revealed that velocity slip positively affects the velocity profile, but the thermal slip negatively impacts the thermal profile. The skin friction coefficient is reduced for increasing value of velocity slip while the thermal slip enhancement also minimizes the heat transfer rate. Even though radiation parameter elevates the temperature profile, the heat transfer rate is declined as this parameter is increased in value. These findings provide valuable insights into the thermal behaviour of ternary hybrid nanofluids, offering potential advancements in aviation cooling, engines, and aerospace applications.

Keywords: Kerosene-based nanofluid, Velocity slip, Thermal slip, Radiation effect

INTRODUCTION

Nanofluid is a top selection of thermal transport fluid in the science and technology field, due to its excellent thermophysical properties (thermal conductivity and rheological properties). The thermophysical properties of the original fluid are enhanced when the nanoparticles submerge into

this fluid, to form a nanofluid. Most of the nanofluid applications prove that the downscaling of particles in nano size offers a better thermal conductivity and heat transport performance, as reported by Sundar et al. (2017), Mikkola et al. (2018) and Salman et al. (2020). The innovations in nanofluid have significant contributions to developing improved efficiency in the fields of electronics cooling (Bahiraei and Heshmatian, 2018; Hamad et al., 2024) and machining process (Kadirgama, 2021). Bahiraei & Heshmatian (2018) has reported that nanofluid delivers better performance as electronic coolants compared to traditional coolants. The heat resistance towards heat sink is enhanced when using nanofluid. In addition, a uniform temperature can be maintained on the surface of the electronic processors. Hamad et al. (2024) remarked that usage of Al2O3 nanoparticles have elevated the cooling ability of the automobile radiator by 17.46%. They also hinted that iron oxide nanoparticles are more efficient than magnetic nanoparticles. Kadirgama (2021) stated that addition of nanoparticles lubricates the cutting zone more effectively thus lessening the frictional force. It has been reported that incorporating nanoparticles in machining process has countless benefits including reduction of cutting force, lowering of surface roughness, maintenance of the tool's hardness and sharpness and increased life of the tool.

Hybrid nanofluid is the nanofluid innovations that can be achieved by hybridising two different nanoparticles. At the same time, hybrid nanofluid has thermophysical properties of two different nanoparticles, subsequently improving the properties of the nanofluid itself. The aim of implementing hybrid nanofluid is to optimize the thermal properties of the original fluid due to the perfect proportion rate among two different nanoparticles. The recent examples of two different nanoparticles in a hybrid nanofluid are alumina-copper: Al_2O_3/Cu (Ghosh and Mukhopadhyay, 2020; Mohd et al., 2022; Isa et al., 2023), magnetite-cobalt ferrite: Fe_3O_4/$CoFe_2O_4$ (Thohura and Moll, 2025), multiwalled carbon nanotubes-zinc oxide: MWCNT/ZnO (Barewar et al., 2025), silver-magnesium oxide: Ag/MgO (Huda et al, 2024), etc. Hybrid nanofluid has wide applications in heat transfer-related industries such as heat exchangers (Huang et al., 2016) and heat sinks (Kumar & Sarkar, 2018). Huang et al. (2016) utilized Al_2O_3-MWCNT/water hybrid nanofluid to explore the pressure drop and heat transfer rate in a chevron plate heat exchanger. They compared the results for conventional fluid (water), nanofluid (Al_2O_3/water) and hybrid nanofluid (Al_2O_3-MWCNT/water). Amongst these, hybridised fluid generated the highest thermal exchange rate. Kumar & Sarkar (2018) conducted numerical study for the flow of nanofluid and hybrid nanofluid passing a minichannel heat sink. They have remarked that the incorporation of nanoparticles enhances the thermal exchange and elevates the pressure drop. They also highlighted that the increment in heat transfer is better for hybrid nanofluid (Al_2O_3-MWCNT/water) compared to nanofluid (Al_2O_3/water). Many factors highly contribute to the heat transfer enhancement of hybrid nanofluids such as base fluid selection, nanoparticles size and shape, nanoparticles dispersion, purity of nanoparticles, preparation method, and compatibility between the nanoparticle's combination (Li et al., 2009).

In continuation of research on nanofluids, further improvements have been made by preparing three different nanoparticles in the single base fluids. This nanofluid is classified as a trihybrid or ternary hybrid nanofluid. Compared to the previous categories of nanofluids, the ternary type has performed excellent thermophysical properties in theoretical and experimental works (Adun et al, 2021). Some of the related ternary type of nanofluid reported in literature are listed as, copper-alumina-titanium dioxide: Cu/Al_2O_3/TiO_2 (Das and Patgiri, 2025); molybdenum disulfide-titanium dioxide-silver: MSO_2/TiO_2/Ag (Ali et al., 2024), single-walled carbon nanotubes-magnetite-copper oxide: SWCNT/Fe_3O_4/CuO (Hemmat et al., 2024), alumina-zinc oxide-magnetite: Al_2O_3/ZnO/Fe_3O_4 (Maifi et al., 2024), titanium dioxide-magnesium oxide-graphene: TiO_2/MgO/GO (Najafpour et al., 2024), etc.

Suction, slip boundary conditions and thermal radiation play crucial role in modifying the flow and heat properties of boundary layer flow. For example, suction plays a role in stabilizing the flow and controlling the boundary layer bifurcation especially in the compressing flow (Hussein et al., 2025). Alharbi (2024) focused on the stagnant zones of the TiO_2-Ag-ZnO ternary hybrid nanofluid flowing over an elongating or compressing sheet by incorporating the suction and velocity slip effects. The author reported that increment in the slip parameter enhances the average velocity profile whereas increment in suction effect decreases the average temperature profile which can be beneficial in cooling processes. Wahid et al. (2024) studied the unsteady flow of Al_2O_3-Cu-TiO_2/water over a biaxially shortening sheet with the effects of suction and thermal radiation. They discovered that a 4% upsurge in suction parameter delays the boundary layer bifurcation by 9%. They also mentioned that a significant rise in temperature is noticeable when the radiation parameter is increased. Eswaran and Kumar (2025) investigated the rotational flow of Cu-SiO_2-TiO_2/water ternary hybrid nanofluid over a stretching or shrinking sheet with the effects of suction/injection, magnetohydrodynamics and melting boundary conditions. They remarked that injection aided thermal transport by decreasing the boundary layer thickness. Additionally, they pointed out that suction encourages heating on the wall thus increasing the boundary layer thickness. Hussein et al. (2025) produced the quantitative note that 1% increment in suction enhanced the skin friction coefficient by 4.17% in the Al_2O_3-Cu-SiO2/water and Al_2O_3-Cu-TiO_2/water ternary hybrid nanofluids over a shortening disc. The time-dependent flow of CuO-MgO-TiO_2/water over a shrinking/stretching wedge is explored by Ouyang et al. (2025). It has been reported that the boundary layer separation is delayed as the suction or injection parameter is increased.

The objective of this study is to extend the work of Ghosh & Mukhopadhyay (2020), by innovating their model from hybrid nanofluid to ternary type of nanofluid. This study aims to fill the gap by altering the nanofluid into ternary hybrid nanofluid and incorporating the thermal radiation effect to the energy equation. In addition, previous researchers compared the nanofluid performance with two types of base fluid which is water and kerosene oil. This study only focuses on kerosene oil as the base fluid. The nanoparticles that are being selected in our model are alumina, copper, and graphene. These three nanoparticles are commonly used nanoparticles, each offering unique benefits in the aspects of thermal conductivity, stability, electrical properties, and so on. Alumina has moderate thermal conductivity and does not easily agglomerate (Timofeeva et al., 2007). Besides, copper has remarkably high thermal conductivity and excellent electrical conductivity (Zhong et al., 2025). Moreover, properties such as ultra-high thermal conductivity, great electrical conductivity, high surface area, lightweight, non-corrosive & chemically stable are offered by graphene (Yusaf et al., 2022). The advantages of kerosene oil as a base fluid are it is a better option where water is not ideal, it has low viscosity but high thermal stability (Wang, 2001). This specific ternary combination of Al_2O_3-Cu-Graphene is not considered by any other previous studies except for Anitha (2024). The novelty of current model compared to Anitha (2024) are: 1) The author used water as the base fluid whereas the current study uses kerosene as the base fluid, 2) The author considered a cylindrical pipe as the flow geometry whereas current paper studies the flow over a flat compressing sheet, 3) The author analysed the entropy generation while the current paper analyses the flow and thermal properties with the additional effects of slip conditions and radiation, and 4) The author used Computational Fluid Dynamics (CFD) method to solve the model whereas numerical method by utilizing MATLAB bvp4c approach is used in current study. Overall, this study examines the effects of suction, velocity slip, thermal slip, and radiation on flow behaviour and heat transfer rate. The governing momentum and thermal energy equations are formulated and transformed into a system of ordinary differential equations through similarity transformation techniques. Numerical solutions are obtained using MATLAB to evaluate key parameters such as the skin friction coefficient and local Nusselt number.

MATHEMATICAL FORMULATION

Partial differential equations and boundary conditions

The two-dimensional boundary-layer flow of ternary hybrid nanofluid is displayed in Figure 1, which is bounded by horizontal shrinking sheet. By considering alumina (Al_2O_3), copper (Cu), graphene as nanoparticles, the governing equations are shown below (Ghosh et al., 2020).

$$\frac{\partial p}{\partial x}+\frac{\partial q}{\partial y}=0, \tag{1}$$

$$p\frac{\partial p}{\partial x}+q\frac{\partial p}{\partial y}=v_{thnf}\frac{\partial^2 p}{\partial y^2}, \tag{2}$$

$$p\frac{\partial T}{\partial x}+q\frac{\partial T}{\partial y}=\frac{k_{thnf}}{(\rho c_p)_{thnf}}\frac{\partial^2 T}{\partial y^2}-\frac{1}{\left(\rho c_p\right)_{thnf}}\frac{\partial q_r}{\partial y}. \tag{3}$$

The velocity components in the x and y directions are denoted by p and q, respectively. Besides, the subscript *thnf* in all the symbols above is defined as ternary hybrid nanofluid. Then, $v_{thnf}=\mu_{thnf}/\rho_{thnf}$ is the kinematic viscosity of the ternary hybrid nanofluid, μ_{thnf} is dynamic viscosity, ρ_{thnf} denotes the density, T denotes the temperature, k_{thnf} is thermal conductivity, and the specific heat capacitance is $(c_\rho)_{thnf}$.

Subsequently, radiative flux can be expressed simply as $q_r=(-4\sigma/3k^*)(\partial T^4/\partial y)$, where σ represents the Stefan-Boltzmann constant and $k^*$is the coefficient of mean absorption. Then, T^4 can be expressed as $T^4\approx 4T_\infty^3T\approx 3T_\infty^4$ by implemeting Taylor series until power law index of T reaches four only. As a result, Equation (3) becomes,

$$p\frac{\partial T}{\partial x}+q\frac{\partial T}{\partial y}=\left(\frac{k_{thnf}}{(\rho c_p)_{thnf}}+\frac{16\sigma T_\infty^3}{3(\rho C\rho)_{thnf}k^*}\right)\frac{\partial^2 T}{\partial y^2}. \tag{4}$$

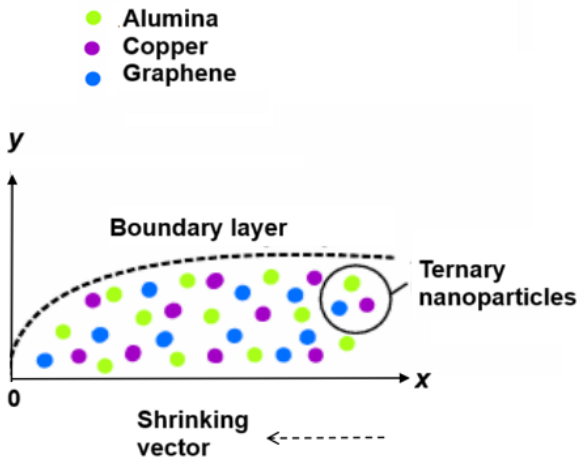

Figure 1: The graphical illustration of the fluid flow model.

The boundary conditions are governed with the effects of partial slip and suction, which can be expressed as:

$$\text{At } y = 0; \quad p = -P_w + V_s' v_f \, (\partial p/\partial y), q = -q_w = -q_0 e^{\left(\frac{x}{2L}\right)}, T = T_w + T_s'(\partial T/\partial y),$$

$$\text{As } y \to \infty; \quad u \to 0, T \to T_\infty. \tag{5}$$

In the above equation, the shrinking velocity is $P_w = ce^{\left(\frac{x}{2L}\right)}$ with $c < 0$, q_0 in $q_w = q_0 e^{\left(\frac{x}{2L}\right)}$ indicates as suction when $q_0 > 0$ and blowing when $q_0 < 0$, and the temperature function at the sheet is expressed as $T_w = T_\infty + T_0 e^{\left(\frac{x}{2L}\right)}$ with T_0 being a constant. The velocity and thermal slip factors are denoted by V_s' and T_s', respectively. Subsequently, $V_s' = V_{s_1} e^{\left(-\frac{x}{2L}\right)}$ and $T_s' = T_{s_1} e^{\left(-\frac{x}{2L}\right)}$, where V_{s_1} and T_{s_1} are positive constant.

The formulation for ternary hybrid nanofluid and the values of thermophysical properties

The formulation of nanofluid properties such as viscosity, density, heat capacity, and thermal conductivity with the ternary nanoparticles are shown in Table 1. Besides, the thermophysical values for density, heat capacity, and thermal conductivity for each type of nanoparticles and base fluid are displayed in Table 2.

Table 1: Related formulations for ternary hybrid nanofluids

Properties	**Ternary Hybrid Nanofluid**
Viscosity	$\mu_{thnf} = \frac{\mu_f}{(1-\phi_1)^{2.5}(1-\phi_2)^{2.5}(1-\phi_3)^{2.5}}$
Density	$\rho_{thnf} = (1-\phi_1)\left\{(1-\phi_2)\left[(1-\phi_3) + \phi_3\frac{\rho_3}{\rho_f}\right] + \phi_2\frac{\rho_2}{\rho_f}\right\} + \phi_1\left(\frac{\rho_1}{\rho_f}\right)$
Heat Capacity	$(\rho c_\rho)_{thnf} = (1-\phi_1)\left\{(1-\phi_2)\left[(1-\phi_3) + \phi_3\frac{(\rho c_\rho)_3}{(\rho c_\rho)_f}\right] + \phi_2\frac{(\rho c_\rho)_2}{(\rho c_\rho)_f}\right\} + \phi_1\left[\frac{(\rho c_\rho)_1}{(\rho c_\rho)_f}\right]$
Thermal Conductivity	$\frac{k_{thnf}}{k_{hnf}} = \frac{k_3 + 2k_{hnf} - 2\phi_3(k_{hnf} - k_3)}{k_3 + 2k_{hnf} + \phi_3(k_{hnf} - k_3)}$; $\frac{k_{hnf}}{k_{nf}} = \frac{k_2 + 2k_{nf} - 2\phi_2(k_{nf} - k_2)}{k_2 + 2k_{nf} + \phi_2(k_{nf} - k_2)}$; $\frac{k_{nf}}{k_f} = \frac{k_1 + 2k_f - 2\phi_1(k_f - k_1)}{k_1 + 2k_f + \phi_1(k_f - k_1)}$

Table 2: Thermophysical values for nanoparticles and base fluid (Alwawi et al., 2022; Choudhary et al., 2023; Jamrus at al., 2024)

Properties	Al_2O_3	Cu	Graphene	Kerosene Oil
ρ (kg/m^3)	3970	8933	2200	783
C_ρ (J/kg K)	765	385	790	2090
k (W/m K)	40	400	5000	0.15

In Table 1, ϕ is the solid volume fraction of nanoparticles, where ϕ_1 is the solid volume fraction for Al_2O_3, ϕ_2 for Cu, and ϕ_3 for graphene. Besides, the subscript *hnf, nf,* and *f* is defined as hybrid nanofluid, nanofluid, and base fluid, respectively.

Similarity Transformations

Stream function, Ψ used to derive the velocities in *x*-axis $\left(p = \frac{\vartheta \Psi}{\vartheta y}\right)$ and y-axis $\left(q = -\frac{\vartheta \Psi}{\vartheta x}\right)$ is defined below. In addition, the following similarity transformation are introduced:

$$\Psi = \sqrt{2\upsilon_f L c} f(\eta) e^{\left(\frac{x}{2L}\right)}, \qquad \eta = y\sqrt{\frac{c}{2\upsilon_f L}} e^{\left(\frac{x}{2L}\right)}, \qquad T = T_\infty + T_0 e^{\left(\frac{x}{2L}\right)} \theta(\eta), \tag{6}$$

where υ_f is the kinematic viscosity of fluid, L is the characteristic length of the shortening sheet, f is the non-dimensional stream function, η is the similarity variable for boundary layer thickness and θ is the non-dimensional temperature function.

Derivation of ODE for conservation of momentum and energy

To convert momentum equation into the ordinary differential equation, we need to substitute Equation (6) into Equations (2) and (4). As a result, momentum equation becomes,

$$\frac{1}{A} f''' + f f'' - 2f'^2 = 0, \tag{7}$$

where $A = [(1-\phi_1)^{2.5}(1-\phi_2)^{2.5}(1-\phi_3)^{2.5}][(1-\phi_1)\left[(1-\phi_2)\left[(1-\phi_3) + \phi_3\left(\rho_3/\rho_f\right)\right] + \phi_2\left(\rho_2/\rho_f\right)\right] + \phi_1\left(\rho_1/\rho_f\right)]$.

With the substitution of Equation (6) into Equation (4), energy equation will transform to,

$$\frac{B}{C}\left[1 + \frac{4}{3}\frac{Rd}{B} Rd\right]\theta''(\eta) + Pr[f\theta' - f'\theta] = 0, \tag{8}$$

where Rd is the radiation parameter, Pr is the Prandtl number of the base fluid, B and C are defined as below,

$$B = k_{thnf}/k_f,$$
$$C = (1-\phi_1)\left[(1-\phi_2)\left[(1-\phi_3) + \phi_3\left((\rho c_\rho)_3/(\rho c_\rho)_f\right)\right] + \phi_2\left((\rho c_\rho)_2/(\rho c_\rho)_f\right)\right] + \phi_1\left((\rho c_\rho)_1/(\rho c_\rho)_f\right).$$

Derivation of ODEs for boundary conditions

The similarity variables in Equation (6) are used to convert Equation (5) into ODE form, and the transformed boundary conditions are presented as Equation (9).

$$\begin{aligned} &\text{When } \eta = 0; && f(\eta) = S, f'(\eta) = -1 + V_s f''(\eta), \theta(\eta) = 1 + T_s\theta'(\eta), \\ &\text{As } \eta \to \infty; && u \to 0, \quad T \to T_\infty, \end{aligned} \tag{9}$$

where $S = -q_0/\sqrt{cv_f/2L}$ is the suction parameter, $V_s = V_{s_1}\sqrt{c/2v_fL}$ is the velocity slip parameter and $T_s = T_{s_1}\sqrt{c/2v_fL}$ is the temperature slip parameter.

Physical Parameters

The skin friction coefficients, C_f and the local Nusselt number, Nu_x are the physical parameters in practical applications, which are defined as,

$$C_{fx} = \frac{\tau_w}{\rho_f p_w^2}, \qquad Nu_x = -x\frac{xq_w}{k_f(T_w - T_\infty)}, \tag{10}$$

with,

$$\tau_w = \mu_{thnf}\left(\frac{\partial p}{\partial y}\right)_{y=0} \text{ and } q_w = -\left(\frac{k_{thnf}}{k_f} + \frac{18\sigma T_\infty^3}{3kk_f}\right)\left(\frac{\partial T}{\partial y}\right)_{y=0}, \tag{11}$$

where τ_w and q_w are the shear stress and heat flux, respectively. Finally, skin friction coefficient and local Nusselt number will have the new form, after Equations (6) and (11) are substituted into Equation (10):

$$\sqrt{Re_x}C_{fx} = D\, f''(0), \qquad \frac{Nu_x}{\sqrt{Re_x}} = B\, \theta'(0), \tag{12}$$

where $D = \mu_{thnf}/\mu_f$ and $Re_x = p_w L/v_f$ is the Reynold's number.

Numerical Solution

Subsequently, the governing Equations (7) and (8), and along with the boundary conditions in Equation (9), are solved in the MATLAB bvp4c solver. To effectively solve this boundary value problem, the equations must be transformed into the first-order ordinary differential equations. Therefore, the following declaration is introduced:

$$\begin{aligned} f = y(1), \qquad f' = y(2), \qquad f'' = y(3), \\ \theta = y(4), \qquad \theta' = y(5). \end{aligned} \tag{13}$$

Equation (7) is written as:

$$f''' = y'(3) = -A[y(1) * y(3) - 2 * y(2) * y(2)]. \tag{14}$$

While Equation (8) is reduced and written as:

$$\theta'' = y'(5) = -\frac{1}{\frac{B}{C}\left[1 + \frac{4}{3}\frac{Rd}{B}Rd\right]} * Pr * \big(y(1)y(5) - y(2)y(4)\big). \tag{15}$$

And the boundary conditions became:

$$\begin{aligned} ya(1) = S, \qquad ya(2) - V_s * y(3) + 1, \qquad ya(4) - T_s * y(5) - 1, \\ yb(2) \to 0, \qquad yb(4) \to 0. \end{aligned} \tag{16}$$

The values of the governing parameters, including suction, radiation, and slip conditions (velocity and thermal) are fixed in the bvp4c function, to obtain the numerical results which satisfy the boundary conditions. The graphical results obtained from MATLAB bvp4c are velocity and temperature profiles, whereas the numerical values obtained from this coding are skin friction coefficient and the local Nusselt number (Equation (12)).

RESULTS AND DISCUSSION

The effects of several parameters on the profiles (skin friction coefficient, $\sqrt{Re_x}C_{fx}$, local Nusselt number, $Nu_x/\sqrt{Re_x}$, velocity profile $f'(\eta)$, and temperature profile $\theta(\eta)$) are presented in graphical forms through Figures 2 to 7. The volume fractions of the nanoparticles used are $\varphi_1 = 0.1, \varphi_2 = 0.04$ and $\varphi_3 = 0.06$. The numerical analysis considers a Prandtl number of Pr = 22.85, which is representative of the kerosine oil and remains fixed throughout the investigation. Other fixed values in the MATLAB coding, unless being mentioned otherwise are S = 2.5, $V_s = 0.1$, $T_s = 1.0$, and Rd = 1.5. To verify the accuracy of the results obtained in this study, Table 3 and Table 4 show the numerical values of the reduced skin friction coefficient $f''(0)$ and the temperature gradient $-\theta'(0)$ for different values of velocity slip parameter V_s when $S = 3.0, Pr = 0.7$, $Ts = Rd = \varphi_1 = \varphi_2 = \varphi_3 = 0$. This table shows good compliment with the available results published by Ghost et. al (2019).

In this paper, only the physical meaning for the first numerical solution will be described, because the first solution (solid line) is the stable and dependable in the actual fluid situation (Ghosh *et al.*, 2020; Isa *et al.*, 2023). Since the stability analysis have been described by the previous study regarding the exponentially compressing sheet in the nanofluid (Ghosh *et al*., 2020), then this paper extends the research focusing on ternary nanoparticles only.

Table 3: Comparison of results for $f''(0)$ for various V_s with $S = 3.0, Pr = 0.7$, $Ts = Rd = \varphi_1 = \varphi_2 = \varphi_3 = 0$

Velocity slip parameter V_s	Ghosh & Mukhopadhyay (2020)		Present study	
	1st Solution	2nd Solution	1st Solution	2nd Solution
0	2.39082	- 0.97223	2.39085	-0.97213
1	0.74131	- 0.27489	0.74127	-0.27489
2	0.42711	- 0.15835	0.42702	-0.15833
3	-	-	0.29948	-0.11106
4	-	-	0.23053	-0.08550
5	-	-	0.18737	-0.06950

Table 4: Comparison of results for $\theta''(0)$ for various V_s with $S = 3.0, Pr = 0.7$, $Ts = Rd = \varphi_1 = \varphi_2 = \varphi_3 = 0$

Velocity slip parameter V_s	Ghosh & Mukhopadhyay (2020)		Present study	
	1st Solution	2nd Solution	1st Solution	2nd Solution
0	1.77124	0.84832	1.77183	0.84774
1	2.02635	0.85911	2.02649	0.85884
2	2.05921	0.86573	2.05929	0.86548

3	-	-	2.07190	0.86853
4	-	-	2.07857	0.87027
5	-	-	2.08270	0.87138

Velocity profile

Velocity profile is plotted against momentum boundary layer thickness, for various values of velocity slip ($V_s = 0.1, 0.4, 0.7$), as shown in Figure 2. It is found that the increase in the velocity slip leads to a rise in the velocity for the first solution near the boundary. The existence of the velocity slip causes the fluid to start with a nonzero velocity at the sheet. As a result, the entire velocity profile is upward. Meanwhile, at the early stage, the velocity decreases for the second solution as the momentum boundary layer thickness increases, but the profile starts to rise again when the thickness increases.

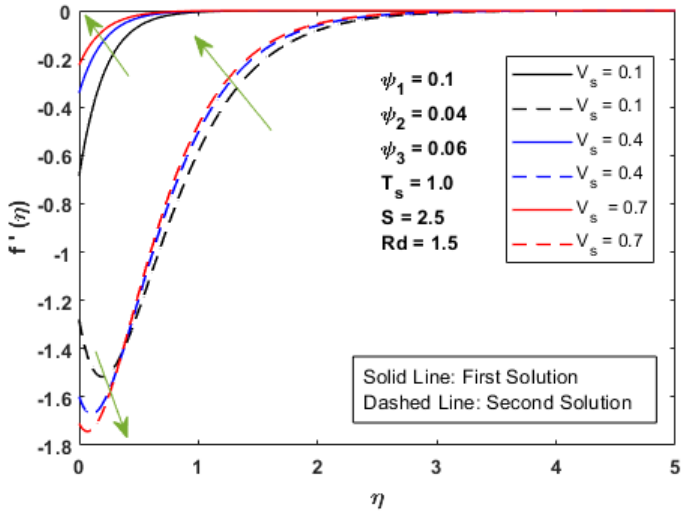

Figure 2: The velocity profile for effect of V_s

Temperature Profile

Next, the effect of thermal slip ($T_s = 1.0, 1.5, 2.0$), on the temperature profile is illustrated in Figure 3. From this figure, there is decrement in first solution as the value of T_s increases. Thermal slip causes a temperature jump at the sheet, which decreases the temperature difference near the sheet. This leads to a flatter temperature profile across the nanofluid area. Meanwhile, the increment in second solution is observed as the value of thermal slip is increased. It shows that the first solution represents a more stable thermal boundary layer.

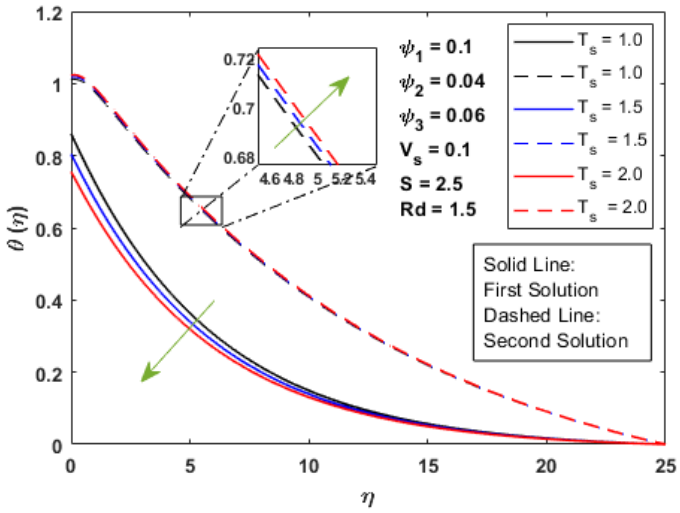

Figure 3: The temperature profile for the effect of T_s

Then, the effects of radiation parameters ($Rd = 1.5, 5.0, 8.0$) on the temperature profile are displayed in Figure 4. It is found that the increasing *Rd* causes the temperature to be increased in both first and second solution which thickens the thermal boundary layer. Radiation increases the temperature profile by injecting thermal energy into the nanofluid, either at the boundaries or throughout the nanofluid area. Therefore, radiative heat transfer enhances heating, leading to elevated temperature levels.

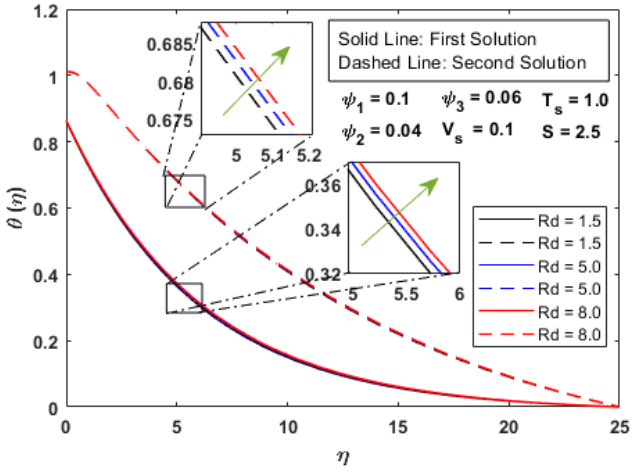

Figure 4: The temperature profile for the effect of *Rd*

Skin friction coefficient

Skin friction coefficient is plotted versus suction parameter *S* for various V_s, as shown in Figure 5. Velocity slip reduces the skin friction coefficient because it lowers the gradient velocity at the wall, which reduces wall shear stress. Since the skin friction coefficient is directly proportional to wall shear stress, it decreases as a result. In addition, as greater suction is applied, the first solution increases for all three increasing values of V_s. In contrast, the second solution will undergo decrement as the suction force increases. When the value of V_s is 0.1, the first and second solution intersects at critical value point, $S_{Vs=0.1} = 1.50168$. For the value of V_s = 0.4, the intersection of the dual solutions is at the point of suction $S_{Vs=0.4} = 1.30740$. Besides, the value of intersection points for the first and second solution for V_s = 0.7 is 1.18680. It shows that the critical points are moving to the left as the value of V_s is increasing, which means that the critical point is decreasing.

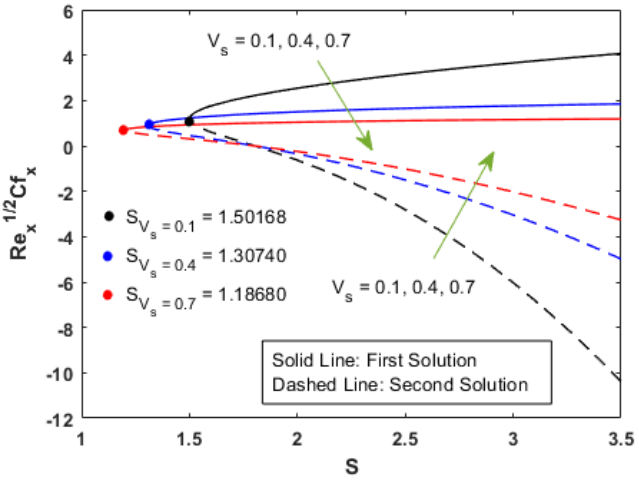

Figure 5: Skin friction coefficient versus S due to the increasing V_s

Local Nusselt number

The variations of local Nusselt number are investigated for thermal slip T_s and radiation parameter Rd. This physical parameter is to quantify the heat transfer rate at the surface. Figure 6 depicts the influence of T_s on the local Nusselt number versus suction, showing that this parameter enhances as T_s rises. Thermal slip reduces the near-wall thermal resistance and flattens the temperature gradient. However, thermal slip increases the temperature difference available for convection. Consequently, even though conduction near the wall is reduced (because of the jump), the nanofluid experiences a larger effective temperature gradient, which can increase convective heat transfer. Moreover, the critical points remain same for various T_s, and the value is 1.50168.

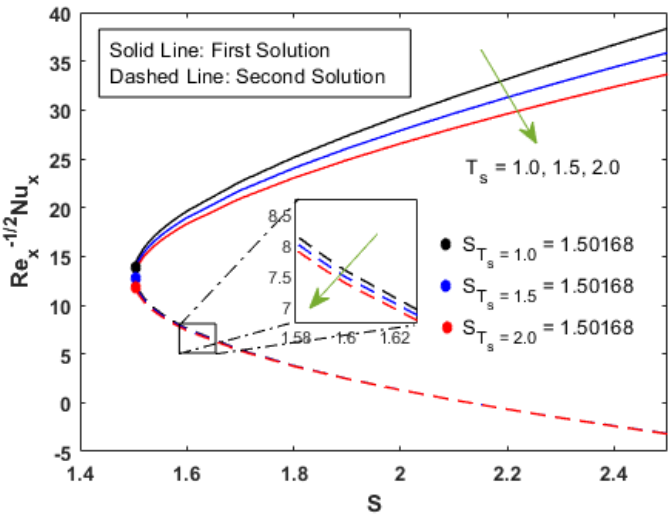

Figure 6: Local Nusselt number versus S due to the increasing T_s

Besides, the radiation also affects the local Nusselt number, which is portrayed in Figure 7. As the radiation parameter increases, the Nusselt number decreases for both the first and second solutions. Even though total heat transfer from the sheet (convective heat + radiation heat) may increase with an intensified radiation, the temperature gradient becomes weaker. This causes the heat transfer portion attributed to convection decreases, causing a drop in local Nusselt number. However, the critical suction parameters remain constant (S_{Rd}=1.50168).

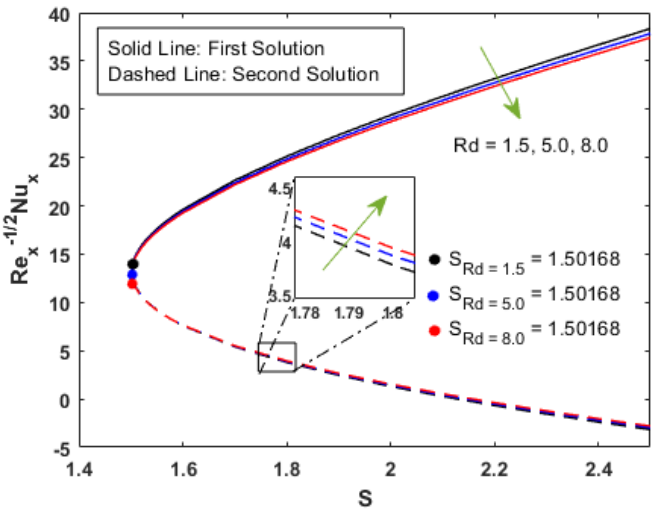

Figure 7: Local Nusselt number versus S due to the increasing Rd

CONCLUSION

This study has provided the flow behaviour and heat transfer characteristics of ternary hybrid nanofluids over a compressing permeable sheet while accounting the radiation and boundary slip effects. By formulating and solving the governing equations using similarity transformations, the partial differential equations have successfully been transformed into ordinary differential equations, which were then numerically solved using MATLAB's bvp4c solver. Overall, this research highlights the crucial role of velocity slip, thermal slip, and radiation effects in influencing the efficiency of ternary hybrid nanofluid flow. The recommendations for future research for this study are including the effect of different nanoparticles shapes , consider specific thermal conductivity model, and extend the original model to three-dimensional fluid flow model. Some of the key findings of this model are pointed out below:

- The stable solution of velocity profile increased when the velocity slip parameter is increased for all the range of η. For the unstable solution, the velocity initially decreases, then started to increase for approximately $\eta > 0.5$.
- The increment in thermal slip and radiation parameter decreases and increases the temperature distribution for the upper branch solution respectively for all range of η.
- For the lower branch solution, the temperature distribution is increased as both the thermal slip and radiation parameters are elevated for all range of η.
- The critical points for the skin friction coefficient move to the left as the velocity slip parameter is increased.
- The critical points for the local Nusselt number remain unchanged for the increment of thermal slip and radiation parameters. Both the parameters deliver same critical point values.

ACKNOWLEDGEMENT

This research was funded by a grant from Universiti Putra Malaysia (Project code: GPI/2023/ 9766100).

REFERENCES

Adun, H., Kavaz, D., & Dagbasi, M. (2021). Review of ternary hybrid nanofluid: Synthesis, stability, thermophysical properties, heat transfer applications, and environmental effects. *Journal of Cleaner Production*, **328**: 129525.

Alharbi, A. A. (2024). Thermal analysis of heat transport in a slip flow of ternary hybrid nanofluid with suction upon a stretching/shrinking sheet. *Case Studies in Thermal Engineering,* **54:** 103965.

Ali, F., Zaib, A., Abbas, M., Anitha, G., Loganathan, K., & Reddy, G. R. (2024). Radiative flow of cross ternary hybrid nanofluid (MoS2, TiO2, Ag/CMC-water) in a Darcy Forchheimer porous medium over a stretching cylinder with entropy minimization. *Heliyon*, **10(14)**:

Alwawi, F. A., Hamarsheh, A. S., Alkasasbeh, H. T., & Idris, R. (2022). Mixed Convection Flow of Magnetized Casson Nanofluid over a Cylindrical Surface. *Coatings,* **12(3)**: 296.

Bahiraei, M., & Heshmatian, S. (2018). Electronics cooling with nanofluids: A critical review. *Energy Conversion and Management*, **172**: 438-456.

Barewar, S. D., Kalos, P. S., Bakthavatchalam, B., Joshi, M., Partil, S., & Sonekar, M. (2025). Analysis and Prediction of Thermo-Physical Properties in water-based MWCNT-ZnO Hybrid Nanofluids Using ANN and ANFIS Models. *International Journal of Thermofluids*, 101159.

Choudhary, S., Mehta, R., Alessa, N., Jangid, S., & Venkateswar Reddy, M. (2023). Thermal Analysis on Kerosene Oil‐Based Two Groups of Ternary Hybrid Nanoparticles (CNT‐Gr‐Fe_3O_4 and MgO‐Cu‐Au) Mix Flow over a Bidirectional Stretching Sheet: A Comparative Approach. *Journal of Engineering*, **2023(1)**: 8828300.

Das, U. J., & Patgiri, I. (2025). Magnetohydrodynamic stagnation flow of Al2O3–Cu–TiO2/H2O ternary nanofluid across a stretching/shrinking cylinder in the presence of nonlinear radiative heat and Arrhenius energy. *Journal of the Korean Physical Society*, **86(3)**: 189-201.

Eswaran, R. & Kumar, M. S. J. (2025). Heat transfer of ternary hybrid nanofluids in a rotating semi-permeable channel with melting and injection/suction. *AIP Advances,* **15:** 035056.

Ghosh, S., & Mukhopadhyay, S. (2020). Stability analysis for model-based study of nanofluid flow over an exponentially shrinking permeable sheet in presence of slip. *Neural Computing and Applications*, **32(11)**: 7201-7211.

Hamad, N. H., Adham, A. M., & Abdullah, R. S. (2024). Cooling electronic components by using nanofluids: a review. *Journal of Thermal Analysis and Calorimetry*, 1-12.

Huang, D., Wu, Z., & Sunden, B. (2016). Effects of hybrid nanofluid mixture in plate heat exchangers. *Experimental Thermal and Fluid Science*, **72**: 190-196.

Hemmat Esfe, M., Hatami, H., Alidoust, S., Toghraie, D., & Sarbaz Karajabad, M. (2024). The volume fraction of nanoparticles and temperature effects on thermal conductivity of SWCNT–Fe_3O_4–CuO/ethylene glycol–water ternary hybrid nanofluid: experimental, numerical, and statistical investigations. *Journal of Thermal Analysis and Calorimetry*, **149(14)**: 7773-7781.

Huda, M. N., Alam, M. S., & Hossain, S. C. (2024). Optimization and sensitivity analysis of hydromagnetic convective heat transfer in a square cavity filled with a porous medium saturated by Ag-MgO/water hybrid nanofluid using response surface methodology. *International Journal of Thermofluids*, 22, 100626.

Hussein, U. N., Khashi'ie, N. S., Arifin, N. M., & Pop, I. (2025). Heat transfer and flow dynamics of ternary hybrid nanofluid over a permeable disk under magnetic field and Joule heating effects. *Frontier in Heat and Mass Transfer.* **23(2):** 1-10.

Isa, S. S. P. M., Parvin, S., Arifin, N., Ali, F., & Ahmad, K. (2023). Soret-Dufour effects on the waterbased hybrid nanofluid flow with nanoparticles of Alumina and Copper. *Malaysian J Math Sci*, **15(19)**: 3419.

Jamrus, F. N., Waini, I., Khan, U., & Ishak, A. (2024). Effects of magnetohydrodynamics and velocity slip on mixed convective flow of thermally stratified ternary hybrid nanofluid over a stretching/shrinking sheet. *Case Studies in Thermal Engineering,* **55(2024)**: 104161.

Kadirgama, K. (2021). A comprehensive review on the application of nanofluids in the machining process. *The International Journal of Advanced Manufacturing Technology*, **115(9)**: 2669-2681.

Kumar, V., & Sarkar, J. (2018). Two-phase numerical simulation of hybrid nanofluid heat transfer in minichannel heat sink and experimental validation. *International Communications in Heat and Mass Transfer*, **91**: 239-247.

Li, H., Ha, C. S., & Kim, I. (2009). Fabrication of carbon nanotube/SiO_2 and carbon nanotube/SiO_2/Ag nanoparticles hybrids by using plasma treatment. *Nanoscale research letters*, **4**: 1384-1388.

Maifi, T., Sari Hassoun, Z., Korei, Z., & Chamkha, A. J. (2024). Exploring enhanced heat transfer in wavy porous enclosures: Optimization and analysis of ternary nanofluid integration under varied boundary conditions with MHD mixed convection. *Numerical Heat Transfer, Part A: Applications*, 1-36.

Mikkola, V., Puupponen, S., Granbohm, H., Saari, K., Ala-Nissila, T., & Seppälä, A. (2018). Influence of particle properties on convective heat transfer of nanofluids. *International Journal of Thermal Sciences*, **124**: 187-195.

Mohd, R. N. D., Isa, S. S. P. M., Arifin, N. M., & Bachok, N. (2022). The thermal properties of water-based hybrid nanofluid (Cu-Al_2O_3) beyond an inclined plane. *Thermal Science*, **26(6 Part A)**: 4561-4570.

Najafpour, A., Hosseinzadeh, K., Kermani, J. R., Ranjbar, A. A., & Ganji, D. D. (2024). Numerical study on the impact of geometrical parameters and employing ternary hybrid nanofluid on the hydrothermal performance of mini-channel heat sink. *Journal of Molecular Liquids*, **393**: 123616.

Ouyang, Y., Basir, M. F. M., Naganthran, K., & Pop, I. (2025). Stability analysis of unsteady ternary nanofluid flow past a stretching/shrinking wedge. *Open Physics,* **23.**

Salman, S., Talib, A. A., Saadon, S., & Sultan, M. H. (2020). Hybrid nanofluid flow and heat transfer over backward and forward steps: A review. *Powder Technology*, **363**: 448-472.

Sundar, L. S., Sharma, K. V., Singh, M. K., & Sousa, A. C. M. (2017). Hybrid nanofluids preparation, thermal properties, heat transfer and friction factor–a review. *Renewable and Sustainable Energy Reviews*, **68**: 185-198.

Timofeeva, E. V., Gavrilov, A. N., McCloskey, J. M., Tolmachev, Y.V., Sprunt, S., Lopatina, L. M., & Selinger, J. V. (2007). Thermal conductivity and particle agglomeration in alumina nanofluids: Experiment and theory. *Physical Review E,* **76**: 061203.

Thohura, S., & Molla, M. M. (2025). Double-diffusive mixed convection and entropy generation of Fe_3O_4-$CoFe_2O_4$-water hybrid nanofluid in an enclosure with a heated wavy cylinder. *Results in Engineering*, **25**: 104345.

Wahid, N. S., Arifin, N. M., Yahaya, R. I., Khashi'ie, N. S., & Pop, I. (2024). Impact of suction and thermal radiation on unsteady ternary hybrid nanofluid flow over a biaxial shrinking sheet. *Alexandria Engineering Journal,* **96:** 132-141.

Wang, T. (2001). Thermophysics Characterization of Kerosene Combustion. *Journal of Thermophysics and Heat Transfer,* **15(2)**.

Wang, X., Song, Y., Li, C., Zhang, Y., Ali, H. M., Sharma, S., ... & Zhou, Z. (2024). Nanofluids application in machining: a comprehensive review. *The International Journal of Advanced Manufacturing Technology*, **131(5)**: 3113-3164.

Wang, X., Wen, Q., Yang, J., Shittu, S., Wang, X., Zhao, X., & Wang, Z. (2023). Heat transfer and flow characteristic of a flat confined loop thermosyphon with ternary hybrid nanofluids for electronic devices cooling. *Applied Thermal Engineering*, **221**: 119758.

Zhong, S., Zhang, X., & Bingyi Zhang, A. L. (2025). Electrical and Thermal Conductivity of Graphene/Copper Composites and Their Applications in High-Efficiency Current-Carrying Conductors: A Review. *Advanced Engineering Materials,* **27(7)**: 2401950.